The Astrophysical Journal Supplement Series, 254:11 (16pp), 2021 May https://doi.org/10.3847/1538-4365/abea20

SpiKeS: Precision Warm Spitzer Photometry of the Kepler Field

Michael W. Werner[1], Varoujan Gorjian[1], Farisa Y. Morales[1], John H. Livingston[2], Grant M. Kennedy[3,4], Rachel L. Akeson[5], Charles Beichman[5], David R. Ciardi[5], Elise Furlan[5], Patrick J. Lowrance[6], Eric E. Mamajek[1], Peter Plavchan[7], Christopher C. Stark[8], and Mark C. Wyatt[9]
[1] Jet Propulsion Laboratory, California Institute of Technology, 4800 Oak Grove Dr., Pasadena, CA 91109, USA
[2] Department of Astronomy, University of Tokyo, 7-3-1 Hongo, Bunkyo-ku, Tokyo 113-0033, Japan
[3] Department of Physics, University of Warwick, Gibbet Hill Road, Coventry, CV4 7AL, UK
[4] Centre for Exoplanets and Habitability, University of Warwick, Gibbet Hill Road, Coventry, CV4 7AL, UK
[5] NASA Exoplanet Science Institute, Caltech/IPAC, Mail Code 100-22, 1200 E. California Blvd., Pasadena, CA 91125, USA
[6] IPAC-Spitzer, MC 314-6, California Institute of Technology, 1200 E. California Blvd., Pasadena, CA 91125, USA
[7] George Mason University, Fairfax, VA 22030, USA
[8] Space Telescope Science Institute, 3700 San Martin Dr., Baltimore, MD 21218, USA
[9] Institute of Astronomy, University of Cambridge, Madingley Road, Cambridge CB3 0HA, UK
Received 2020 October 12; revised 2021 February 18; accepted 2021 February 19; published 2021 April 27

Abstract

The ∼200,000 targets monitored for photometric variability during the Kepler prime mission include the best-studied group of stars in the sky, due both to the extensive time history provided by Kepler and to the substantial amount of ancillary data provided by other investigators or compiled by the Kepler team. To complement this wealth of data, we surveyed the entire Kepler field using the 3.6 and 4.5 μm bands of the Warm Spitzer Space Telescope, obtaining photometry in both bands for almost 170,000 objects. We demonstrate relative photometric precision ranging from better than ∼1.5% for the brighter stars down to slightly greater than ∼2% for the faintest stars monitored by Kepler. We describe the data collection and analysis phases of this work and identify several stars with large infrared excess, although none that is also known to be the host of an exoplanetary system. The final catalog resulting from this work will be available at the NASA Exoplanet Archive.

Unified Astronomy Thesaurus concepts: Stellar properties (1624); Stellar colors (1590); Stellar types (1634); Infrared excess (788); Infrared astronomy (786); Spectral energy distribution (2129); Photometry (1234); Catalogs (205); Surveys (1671); Stellar photometry (1620); Stellar evolutionary tracks (1600)

1. Introduction

During its 4 yr prime mission (2009–2013 May), the Kepler spacecraft (Borucki et al. 2010) produced highly precise time-series photometry for over 175,000 stars, mostly main-sequence dwarfs of types F, G, and K, and for other astronomical targets of all types. These data, together with the ancillary data about the stars available at the NASA Exoplanet Archive and the wealth of additional data produced by surveys of the Kepler field at wavelengths from the X-ray to the mid-infrared, make these the best-studied group of stars in the sky. In addition to the prime application of the Kepler data, which is to search the light curves for transiting exoplanets, the Kepler data have been used for numerous papers on astrophysical phenomena ranging from asteroseismology to reverberation mapping of active galactic nuclei (e.g., Ciardi et al. 2011; Mushotzky et al. 2011; Yu et al. 2018).

The work described here adds to the data on the high-precision photometry of the entire Kepler field using the 3.6 and 4.5 μm bands of the Warm Spitzer Space Telescope's Infrared Array Camera (IRAC; Fazio et al. 2004; Werner et al. 2004). This project is named SpiKeS, which stands for the Spitzer Kepler Survey. We have surveyed the entire Kepler field in Cygnus, which the spacecraft observed for 45 consecutive months, but not any of the areas studied by the successor K2 mission. We succeeded in achieving our objective, which was to achieve a measurement precision on the brightness of the Kepler stars better than the absolute calibration uncertainty of the Spitzer data, estimated to be ∼2.4% (Bohlin et al. 2011; Carey et al. 2012). This was done through precise reduction of the images obtained by Spitzer. There is a separate Spitzer Science Center (SSC) effort to combine all 16 yr of IRAC data into supermosaics with a corresponding source list (tentatively titled the Warm Mission Spitzer Enhanced Imaging Products (WM-SEIP)) to give a mission catalog of images, targets, and photometry. The user can explore this database and then, if desired, dive deeper into removing remaining systematic uncertainties for objects of interest. Overall, we expect similar results for photometry from SpiKeS and WM-SEIP, but SpiKeS will be superior in its precision due to a more refined treatment of systematic uncertainties. Unlike SpiKeS, the WM-SEIP will include most of the ∼13 million sources in the Kepler Input Catalog (KIC), and not just the ∼200,000 monitored for planets by Kepler and included in SpiKeS.

The applications of this and other data being accumulated on the Kepler field are limited only by astronomers' imagination. However, the principal interest of the SpiKeS team, as illustrated below, was to search for infrared excesses that could in principle be due either to circumstellar dust or to cool companions of the Kepler stars. In addition, precise spectral energy distribution (SED) fitting of the SpiKeS and other data, combined with distances measured by Gaia (Gaia Collaboration et al. 2016, 2018), as has been done by Berger et al. (2020), can lead to improved estimates of the radii of exoplanet host stars, which, in combination with the measured transit depths, can also yield the best possible determinations of exoplanet radii.

A note on nomenclature may prove helpful as we discuss our work. The stars for which Kepler reported high-cadence light curves are referred to as Kepler targets. The KIC, from which

the Kepler targets were drawn, includes ∼13 million objects. Although essentially all of these targets are included in SpiKeS measurements of the entire Kepler field, our focus is on the ∼200,000 of these—the Kepler targets—that were monitored continually by Kepler. In this paper all data described and discussed refer either to the Kepler targets or to a subsample of the Kepler targets, and all magnitudes are on the Vega scale.[10] Finally, the plots below include a small number of Kepler targets that are not giant or normal dwarf stars (e.g., galaxies or white dwarfs). We are confident that their presence does not compromise the conclusions of this work.

In Section 2, we describe the experimental design and the data reduction approach; we had to develop novel data reduction procedures because of the brightness of many of the observed stars and the fact that, in most cases, only three observations of a particular star were taken. In Section 3, we present the results, including those of a comparison of two separate epochs of observations of a $2\overset{\circ}{.}5 \times 2\overset{\circ}{.}5$ Kepler test tile (KTT) and other comparisons that validate our experimental design, uncertainty determination, and absolute photometry. In Section 4, we report the results of a preliminary search for infrared excesses among the observed stars, which identified several stars showing substantial excess emission. The results of the work are summarized in Section 5.

The paper also includes several appendices. Appendix A presents our approach to data analysis, including our treatment of systematic effects and elimination of outlying measurements. These include a seldom addressed issue (a column pull-up due to bright sources), which led to overestimates of the flux from a small fraction of the observed stars. Appendices B and C present details related to the execution and scheduling of the observations. In Appendix D we discuss evidence for variability among the Kepler targets.

The Wide-field Infrared Survey Explorer (WISE) mission (Wright et al. 2010) included the Kepler field in its all-sky survey. The WISE data on the Kepler field have been analyzed and discussed by Kennedy & Wyatt (2012). Their main objective was to search for excesses in WISE bands 3 and 4 at 12 and 22 μm, but they did discuss WISE photometry of the Kepler field in shorter-wavelength bands at 3.4 and 4.6 μm, roughly analogous to the Warm Spitzer bands. In Appendix E we compare Spitzer and WISE photometry of the Kepler targets. Our principal conclusion is that because the Spitzer pixels are one-tenth the angular area of WISE's, there are an appreciable number of sources reported as single by WISE that prove to be double when observed by Spitzer. In Appendix F, we present and discuss a Hertzsprung–Russell (HR) diagram for the observed stars, using absolute magnitudes based on distances derived from Gaia.

2. Observations

We began this work with a pilot project in 2013 January, during Spitzer Cycle 9 [PID 90100], by observing a KTT, which is one of the twenty-one $2\overset{\circ}{.}5 \times 2\overset{\circ}{.}5$ sectors into which the full Kepler field is divided. The test field is centered at $\alpha = 292\overset{\circ}{.}765220$ and $\delta = 42\overset{\circ}{.}08020$ (J2000).

2.1. Construction of Astronomical Observation Request

The experimental design of the pilot project allowed complete coverage of the KTT with both the 3.6 and the 4.5 μm IRAC 256×256 pixel arrays, which view adjacent $\sim 5' \times 5'$ fields of view (FOVs) on the sky with $\sim 1\overset{''}{.}2$ pixels and a point-source FWHM of $\sim 1\overset{''}{.}8$-to-$2\overset{''}{.}0$. Observations of the tile were carried out using the IRAC mapping mode in array coordinates, so that the scans and steps were parallel to rows or columns of the arrays. They were planned by dividing the tile into a series of strips of sizes of $\sim 0\overset{\circ}{.}5 \times 2\overset{\circ}{.}5$. An astronomical observation request (AOR)—a script that defines a Spitzer observation—was constructed for each strip, which mapped it in both IRAC bands by scanning in the long direction along one side of the strip, stepping just under one array-width perpendicular to the long direction, and returning and repeating until the tile was completely covered. To achieve complete coverage of the KTT, five AORs were chained together to observe the full tile in consecutive Spitzer observations, which took a total of 22 hr. The combined strips are slightly larger than the KTT because the Spitzer FOV rotates on the sky over time.

The selected integration time was 12 s, and the telescope was moved by a little less than a third of the $\sim 5' \times 5'$ FOV in the scan direction between integrations. Thus, most stars were observed three times, resulting in an integration time of 31.2 s, when the overhead due to Fowler sampling is subtracted, as discussed in Section 2.4.2 of the IRAC Handbook.[11] However, the overlap between adjacent scans and AORs led to a few stars being observed up to as many as 10 times, as summarized in Appendix B. We applied severe quality checks during the data reduction process (Appendix A), so that in the end some sources—both in the pilot project and in the final survey discussed below—had only one (or perhaps even zero) useful observation in a particular Spitzer band (Appendix B). Only measurements that survived these quality checks are included in the figures or calculations presented in this paper. Similarly, only such high-quality measurements are included in the archival data stored at the NASA Exoplanet Archive. However, the SpiKeS archive will contain data on all Kepler targets, including those for which SpiKeS provides a measurement at only one (or perhaps neither) of the IRAC bands. This will put the wealth of ancillary data (see Table 4 below) on all Kepler targets into a single, readily accessible database.

The success of the pilot project, which reached our desired photometric precision, encouraged us to propose to observe the entire Kepler field using the same methodology. This main survey was designed similarly to the pilot survey so that each Kepler tile was observed as continuously as Spitzer's scheduling constraints permitted. We observed all 21 Kepler tiles, which included a reobservation of the KTT. A repeat observation of the KTT was critical in allowing us to quantify the precision of our photometry. In the main survey, the observations of a particular tile were typically spread over 2 or 3 days, interrupted as Spitzer slewed away to carry out other observations. The AORs had to be designed to accommodate this spread. The full-field proposal was accepted [PID 10067] and executed, primarily in 2014, according to the schedule compiled in Appendix C.

[10] The Vega-based magnitude zero-points for the IRAC are IRAC1 = 280.9 Jy and IRAC2 = 179.7 Jy.

[11] The IRAC Handbook is available at https://irsa.ipac.caltech.edu/data/SPITZER/docs/irac/.

2.2. Data Reduction and Source Extraction

The pilot project served as a proving ground for the data reduction techniques subsequently adopted for the entire project. In both cases, the data on a given tile was pipeline-processed and calibrated by the SSC and made available to the investigator team for further analysis. The Kepler targets include stars brighter than 10th mag in the two IRAC bands (IRAC1 denotes the 3.6 μm band and IRAC2 the 4.5 μm band), and almost all of the Kepler targets are brighter than 15th mag in both IRAC1 and IRAC2. The nominal saturation limit, according to the IRAC Handbook, for our observations is 10.1 at IRAC1 and 9.4 at IRAC2. However, this is a very conservative limit because it assumes that a star is centered on the saturating pixel. In our effort to provide a reliable database, we used a flag generated for saturated pixels in the reduction pipeline (IRAC Handbook, Section 7.2.1) to remove saturated sources from our catalog. Note also that the SSC pipeline applies a correction to pixels that approach saturation. A few sources in our final catalog are above the nominal saturation limit but were not flagged by the SSC as saturated likely because of the above-noted conservatism in determining the limit. Because saturated sources are the brightest sources, they are well measured by WISE with high precision, and so a good record of their near-infrared flux exists.

Because of the brightness of the stars, the main source of statistical noise for many of our observations was shot noise in the stellar photons rather than fluctuations in the celestial background (which set the sensitivity limit for Spitzer's deep surveys for faint objects). In this regime, when the stellar photon–limited signal-to-noise ratio can exceed 100:1, Spitzer observations become limited by systematic effects that are not dominant in observations of fainter targets. We therefore employed the additional data reduction steps recommended by the SSC to reduce systematic effects, which were corrected in the individual frames as outlined below and described in detail in Appendix A.

The first step in the analysis of the data on a given tile was to form a mosaic of the pipeline-processed and calibrated data provided by the SSC, using the MOPEX tool available at the SSC. The mosaic was then analyzed using SExtractor (Bertin & Arnouts 1996) to identify point sources. The positional association of these point sources with sources in the KIC allowed us to identify the sources seen by IRAC with those previously identified in the Kepler field. Positional agreement to within 2″ (larger than the positional uncertainty of the SpiKeS data) was required to establish a match. The mosaics were not suitable for precision photometry because they did not incorporate corrections for the systematic effects discussed in detail in Appendix A. Also described in Appendix A are the steps we took to reject outlying measurements, even though in some cases this led to there being no valid measurements for a star at a particular wavelength, because we felt that accuracy was more important than completeness. Appendix B tallies the stars with 0, 1, 2, etc., usable observations for the entire survey.

Following the preparation and analysis of the mosaics, all the individual Corrected BASIC Calibrated Data (CBCD; see Section 5.2 of the IRAC Instrument Handbook) frames in which a particular star appeared were identified (usually 3 but could be up to 10 as noted above). Then photometry was done on the star in each CBCD frame using the IDL routine aper.pro with a 2 pixel (2.″4) photometry radius and a 12–20 pixel radius sky annulus, and the aperture correction recommended by the SSC was applied. The corrections described in Appendix A were applied to determine the flux for that stellar image. The final value for the flux of each star was the median of its individual measurements from the CBCD frames, which makes the magnitudes we report robust against the influence of outlying measurements as the number of measurements per star increases. Some stars were affected by nearby bright sources, but this effect was not the same for both channels. Using the techniques described in Appendix A, we have identified which measurements are suspect and eliminated them from the final catalog.

We estimated the uncertainty in the first measurements of the KTT as follows. We first combined in quadrature the statistical noise of the individual measurements of a given star, as reported by aper.pro, and divided this sum by the number of observations. Because the scatter in the flux determinations for individual stars was generally greater than the expectation based on the statistical noise in each measurement, it was clear that the overall uncertainty in the measurements of the brightest stars was dominated by systematic effects. We accordingly determined the systematic uncertainty for the KTT at each wavelength by identifying the 100 brightest stars with three or more valid measurements in each band in the KTT and calculating the median absolute deviation (MAD) of each individual star's measurement set. We then set the global systematic uncertainty to the median value of these 100 MADs and combined it in quadrature with the statistical uncertainty to determine the measurement error for each star. The final uncertainty using this technique was less than the 2.4% calibration uncertainty that we had set as our objective, which encouraged us to propose the complete survey.

3. Data Validation

3.1. Establishing the Final Uncertainties with Repeated Observations of the KTT

Repeating observations of the KTT in the full Kepler field survey provided us an important opportunity to assess the precision of our photometry. This was particularly important because we found that we were limited by systematic effects that were difficult to quantify in a single visit to a tile. Figure 1 shows histograms of $R = \mathrm{F1}/\mathrm{F2}$ in three magnitude ranges for both IRAC1 and IRAC2, where F1 is the flux measured for a particular star at epoch 1 and F2 the flux measured at epoch 2, following the procedure given in the previous section. The data shown are for 10,742 Kepler targets in the KTT that were detected in both IRAC1 and IRAC2 in both epochs. The widths of the distributions were determined by fitting a Gaussian distribution to the histograms. Note that the ratioing procedure shown in the histograms of Figure 1 increases the dispersion by the square root of 2 over that of a single determination.

The fitted Gaussian sigma values (divided by the square root of 2) for each wavelength band and each magnitude bin are given in the "internal uncertainties" columns of Table 1, which adds the 13–14 mag bin to the data shown in Figure 1. These values reflect the variability of the systematic corrections to the observed flux between the two measurements of the KTT as well as the noise due to Poisson fluctuations of the stellar and sky background photon rates. These values exceed the uncertainties in the measurements of the stellar fluxes at a single epoch. That is, the epoch-to-epoch variation is greater

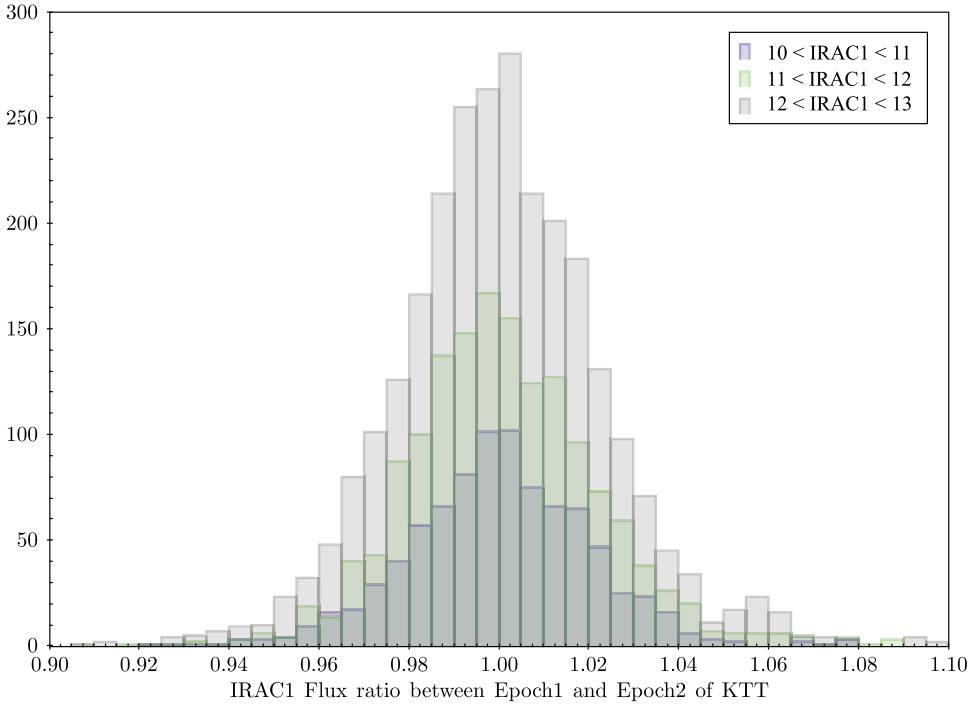

(a)

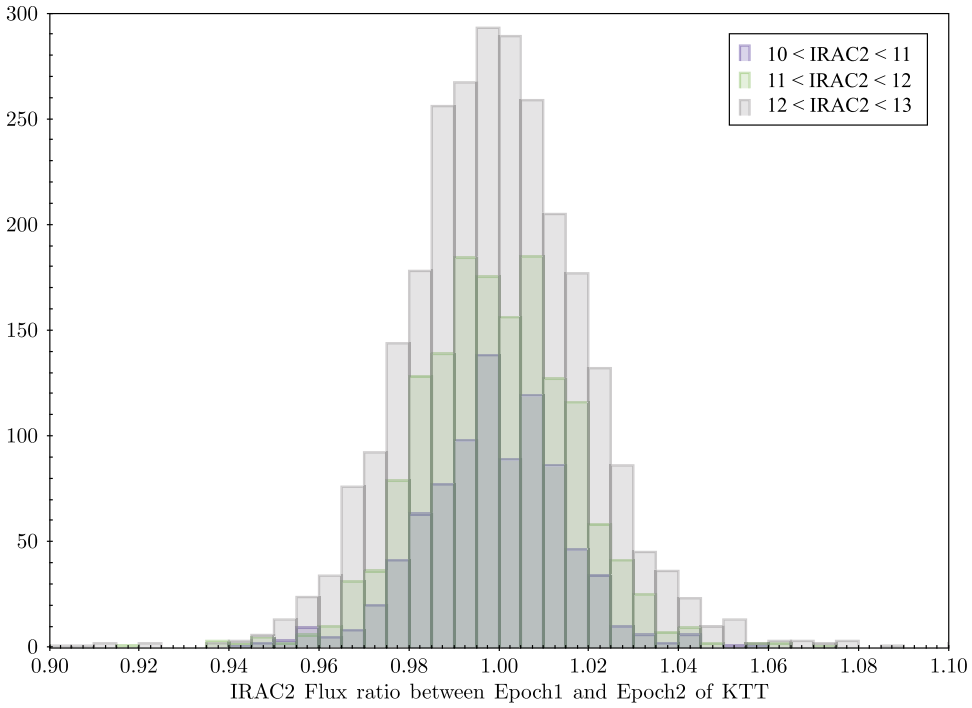

(b)

Figure 1. Histograms showing distribution of IRAC1 (a) and IRAC2 (b) flux ratios for Kepler targets in the KTT from two independent measurements separated by 1 yr. Histograms are shown for three magnitude ranges.

than expected from the measurement at a single epoch. We attribute this to variations in the systematic corrections applied separately to the data at each epoch. We therefore use the internal uncertainties as the basis for an estimate of the uncertainty in the flux determinations for each magnitude range for the entire survey. These values are used, for example, in many of the figures presented below. Note that even for the faintest sources, the "internal uncertainty" is smaller than the overall IRAC absolute calibration uncertainty of ∼2.4% (Carey et al. 2012). For practical applications, the Table 1 "internal uncertainties" should be used when comparing fluxes within this catalog. When using our data together with data taken in

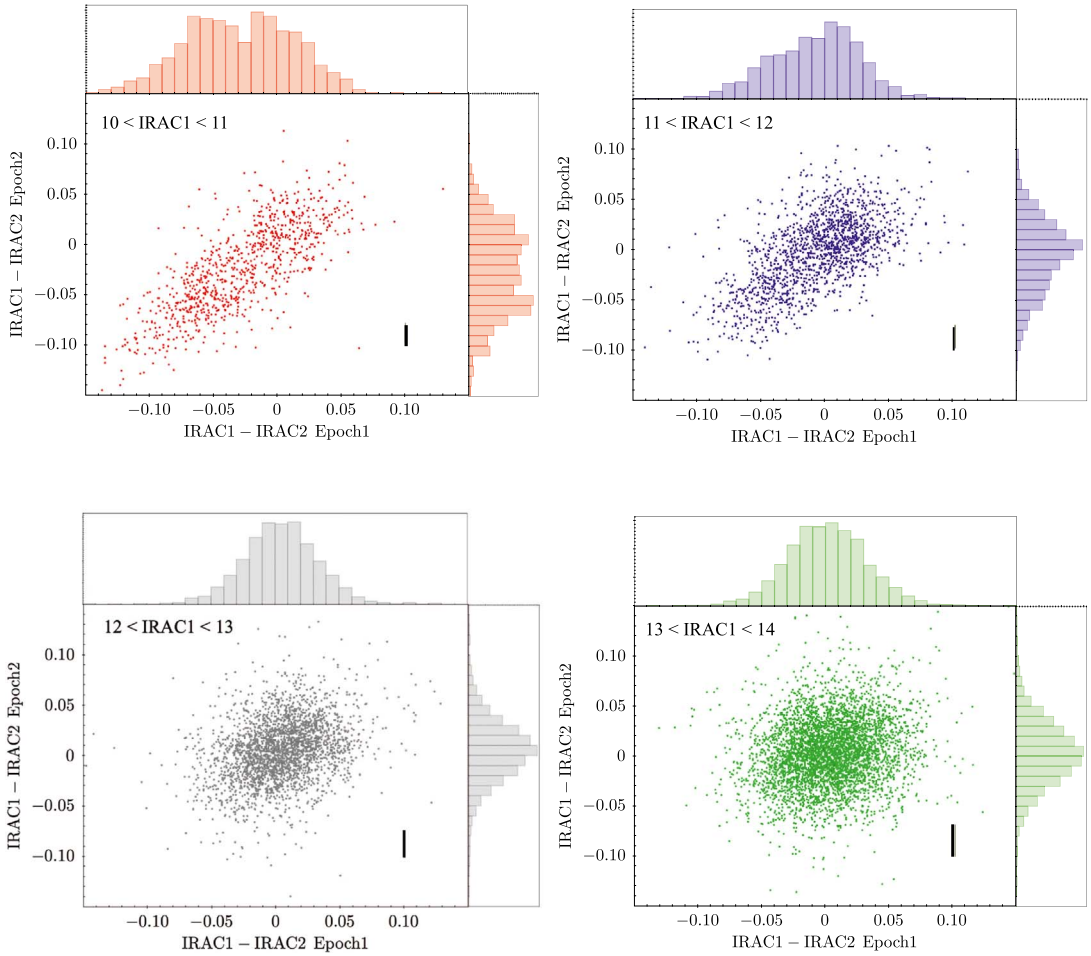

Figure 2. IRAC1–IRAC2 colors are compared for the two epochs of measurement of the KTT. This plot includes all sources within the IRAC1 magnitude range indicated in the upper left corner of each plot at both epochs of the pilot program. The two lobes seen in the upper left plot ($10 < \mathrm{IRAC1} < 11$) are due to dwarf stars (to the red) and giant stars (to the blue). The 1σ uncertainty is given by a bar for each magnitude range and is the same for both axes. The histograms on each axis show the one-dimensional numerical distribution, which is hidden by the crowding of the data points.

Table 1
Uncertainties per Magnitude Bin

Magnitude Bin	No. per Bin	Internal Fractional Flux Uncertainty		External Fractional Flux Uncertainty	
		IRAC1[a]	IRAC2[a]	IRAC1[b]	IRAC2[b]
10–11	870	0.015	0.012	0.028	0.027
11–12	1550	0.017	0.014	0.029	0.028
12–13	2769	0.018	0.017	0.030	0.029
13–14	4777	0.021	0.023	0.032	0.033

Notes.
[a] The internal uncertainties give the median 1σ measurement precision for stars of different magnitude ranges based on the repeatability of observations of 10,742 Kepler targets in the KTT when compared between two epochs. We use these uncertainties for all Kepler targets in our full sample in each magnitude bin, and they can be used for comparing fluxes within this catalog.
[b] The external uncertainties are the quadrature sums of the internal uncertainties with the 2.4% IRAC calibration uncertainty and should be used when comparing our measurements with those made in other spectral bands.

other bands, as is done in fitting stellar models, the 2.4% calibration uncertainty should be added in quadrature, leading to the overall uncertainties given in the "external uncertainties" columns.

The result of the above steps is a final catalog with 174,667 sources having one or more valid measurements at IRAC1 and 179,896 with one or more valid measurements at IRAC2 (see Appendix B). A total of 169,828 sources, or about 88% of all Kepler targets, have valid measurements in both bands. There are 7249 objects with no IRAC observations in either IRAC1 or IRAC2. The majority of those sources (5344) are saturated in the IRAC data. The other objects with no reported SpiKeS measurements are distributed uniformly in magnitude. Of the 7249 Kepler targets without SpiKeS measurements reported, there are 6804 that do have WISE observations, leaving only 445 Kepler targets that do not have any 3–5 μm observations by recent space-based missions.

3.2. Cross-comparison of Stellar Colors for the Two Epochs of the KTT

Further evidence for the quality of the photometry and insight into the nature of the Kepler targets are presented in Figure 2, where we compare the [IRAC1–IRAC2] color measured at the two epochs for the KTT in four magnitude ranges between 10th and 14th mag. Histograms showing the colors measured at each epoch are projected on the appropriate axes. The error bars in these figures are based on the data shown in Table 1. The axes have been truncated to maintain

Table 2
Comparison of Two Independent Photometric Measurements of SpiKeS Data on KIC 8462582

	IRAC1 mag	IRAC2 mag
Photometry from Marengo et al. (2015)	10.477 ± 0.0059	10.437 ± 0.0107
SpiKeS pipeline	10.485 ± 0.015	10.449 ± 0.012

clarity while eliminating a handful of very red sources, presumably active galaxies or highly evolved or very cool stars, from the discussion.

For the brighter stars, shown in the top two plots of Figure 2, the points in the color–color diagram stretch out along a line with a slope = 1. We expect that main-sequence stars will be slightly red in this color index, and attribute the blueward peak or extension to giant stars, including red clump giants, which are expected to be both common and slightly blue in the IRAC bands as they are in the WISE bands (Chen et al. 2014; Li et al. 2016; see also the HR diagram in Appendix F). This identification is validated by the appearance of the corresponding histogram for fainter stars; the extension due to giants is not seen at all for stars with IRAC1 magnitudes fainter than 12 (bottom row of Figure 2). This occurs because the giants are ~1000 times as luminous as main-sequence stars of similar color; at the fainter magnitudes, we would see giants only if they lay high above the galactic plane, where such stars are expected to be relatively rare. We estimate that ~37% of the Kepler targets brighter than 12th mag at 3.6 and 4.5 μm have giantlike colors and do not lie on the main sequence. This is consistent both with the log(g) values of the sources in the Mathur et al. (2017) database and with the luminosities derived from Gaia distances (see Appendix F).

Finally, note that in Figure 2 the dispersion of the data is consistent with the errors shown in Table 1, particularly when it is borne in mind that reddening variations across the field, not accounted for in our analysis, could increase the measured dispersion in [IRAC1–IRAC2] at a single epoch. The reddening estimates in the KIC suggest an average A_V of ~0.5 in the KTT. Taking the reddening curve of Rieke & Lebofsky (1985), this suggests that the distribution of [IRAC1–IRAC2] colors would be widened by more than 0.02, which is significant on the scales of Figure 2.

3.3. KIC 8462852

An additional measure of the precision of the photometry is possible because the unusual Kepler light curve of KIC 8462852, also known as Boyajian's star (Boyajian et al. 2016), drew attention to our data. Table 2 shows a comparison between our SpiKeS pipeline measurements and those of Marengo et al. (2015), who analyzed the SpiKeS photometry on this star with a methodology similar to ours but differing in details. For example, they carried out aperture photometry with a 3 pixel radius and a sky annulus extending from 3 to 7 pixels, as opposed to our photometry with a 2 pixel radius and a sky annulus from 12 to 20 pixels. The excellent agreement (Table 2) of the Marengo et al. (2015) reduction with our pipeline reduction of the same data highlights the accuracy and the precision of our results.

3.4. Absolute Calibration Uncertainty and Model Comparison

We have used our measurements of well-characterized standard stars in the Kepler field, known as "gold" and "platinum" stars, to provide an independent assessment of the quality of Spitzer's absolute calibration. These stars are part of a larger initial sample of 2000 Kepler targets selected by the Kepler Asteroseismic Science Consortium based on their measure of stellar oscillations (Chaplin et al. 2011, 2014; Huber et al. 2011; Verner et al. 2011). To provide the best possible assessment of the calibration, we consider the 67 gold and platinum stars that are detected by SpiKeS in both Spitzer IRAC1 and IRAC2, that have two or more measurements in each band, and that are reliably below the IRAC1 and IRAC2 saturation levels. We compare the predicted and measured IRAC fluxes for these stars.

To carry out the IRAC flux comparison, we adopt a synthetic stellar photosphere model (NextGen model) to predict the stellar emission. The stellar properties (i.e., effective temperature $T_{\rm star}$, log(g), extinction coefficient A_V, metallicity, stellar radius, etc.) are obtained from the California Kepler Survey (Petigura et al. 2017) and/or the DR25 (Mathur et al. 2017) stellar catalogs. The wavelength dependence of interstellar extinction is accounted for by assuming a reddening law of $R_V = 3.1$ (Draine 2003), which accounts for graphite and astronomical silicate grains. Following the lead of Fulton & Petigura (2018), we then pin the stellar model to the Two Micron All Sky Survey (2MASS) K_s-band photometry (Skrutskie et al. 1995) and overplot the IRAC and WISE measurements for comparison. Thus, Figure 3 shows the reddened model photospheres for four representative standard stars, along with our SpiKeS-measured photometry on each. The excellent agreement of the extrapolated stellar model with the SpiKeS data offers us an independent method to assess the uncertainties in the Spitzer calibration.

We have repeated this analysis for each of the 67 gold and platinum stars in our sample. To quantify the accuracy of the SpiKeS flux measurements, we predict the expected IRAC1 and IRAC2 fluxes for each standard star by convolving the IRAC filter response functions with each reddened stellar photosphere model (as was done in preparing Figure 3) and compare these predictions to the Spitzer measurements as calibrated by the SSC. We find that the SpiKeS photometric measurements are in excellent agreement with the predictions. Figure 4 presents histograms of the 67 standard stars as seen by IRAC1 and IRAC2 as a function of the difference between the predicted flux from the stellar model and the observed flux divided by the predicted photosphere flux. Note that the mean of the offset is close to zero for both bands and that the width of the distribution is less than 2.4% in both cases. These results are consistent with the claimed accuracy of the overall Spitzer calibration, which was established by a similar process, also involving 2MASS data but using the spectra of A stars and K giants as the standard stellar spectra. Our results show that the same accuracy can be achieved by using NextGen models as the stellar templates.

The good agreement between models and data indicates that we should be able to detect small IRAC1 and IRAC2 excesses around stars in the Kepler field. Note that none of the 67 Kepler standard stars studied here show signs of excess emission in the IRAC wave bands.

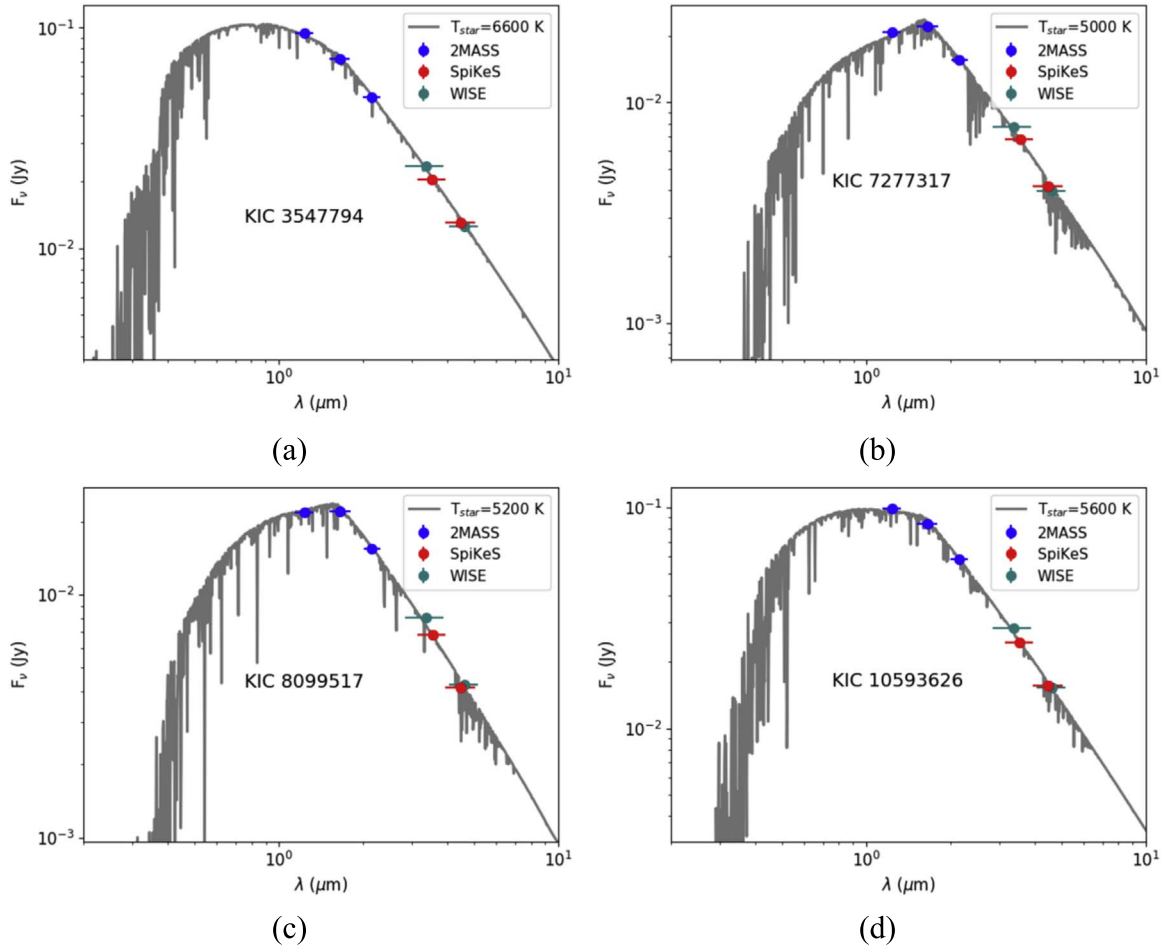

Figure 3. Four sample SEDs of very well studied Kepler standard stars with SpiKeS photometry demonstrate excellent agreement with expectation from the stellar photospheres. KIC 3547794 (upper left) is the hottest star, whereas KIC 7277317 (upper right) is the coolest star in this standard-star sample. The agreement extends across a broad range of reddening factors. For example, the star on the bottom right, KIC 10593626, has the lowest extinction ($A_V \sim 0.1$) in this standard-star sample, whereas the star on the bottom left, KIC 8099517, has the largest reddening effect, with A_V of ∼0.5. The WISE photometry (teal circles) is included for comparison with the SpiKeS measurements. Data like this on a total of 67 Kepler standard-star targets have been used to verify the accuracy of the Spitzer calibration.

4. Searching for Infrared Excesses

Here we report the initial results of a search for large infrared excesses in the SpiKeS data. A more comprehensive analysis extending toward smaller excesses will be presented separately.

4.1. A Search for Infrared Excesses in the Full Sample of Kepler Targets

In many cases, the infrared excess produced either by circumstellar dust warmer than 300 K or by a cool companion would have a roughly thermal spectrum and thus might be seen in both IRAC1 and IRAC2. To test this idea and to show the full scope of the SpiKeS data, we show in Figure 5(a) a *J*-IRAC1 versus *J*-IRAC2 color–color plot for the full sample of 169,741 Kepler targets from the full survey for which we have data in both Spitzer bands and *J* data from 2MASS. The vast majority of the stars in the plot lie on the main sequence, which covers the range $-0.2 < J\text{-IRAC1} < 1.3$ for dwarf stars with spectral types B through M (Pecaut & Mamajek 2013).[12] Objects identified as giants based on $\log(g) < 1.5$ in the Mathur et al. (2017) database are color-coded teal in this figure. Many can be seen as part of the lower fork lying below the main sequence for $J\text{-IRAC1} > 1.0$.

As is shown in Figure 5, sources in the sparse extension to the upper right (red in both *J*-IRAC1 and *J*-IRAC2) are frequently identified in SIMBAD as infrared excess galaxies that have a great amount of warm dust. Many of the stars lying in the sparse extension to the lower left (blue in both *J*-IRAC1 and *J*-IRAC2) are listed as binary stars in SIMBAD; it is possible that they varied in the ∼20 yr between the 2MASS measurement and our Spitzer measurement. We expect an equal number of sources that varied such that their colors extend to the upper right (red in both *J*-IRAC1 and *J*-IRAC2); however, these would be moving along the main sequence and not be easily identifiable on this plot. In Appendix D we show that less than 1% of the Kepler targets varied significantly over the ∼1 yr interval between the two measurements of the KTT, but the number of possible longer-term variables suggested by Figure 5 is far less than 1% of the entire sample.

Figure 6 is a zoomed-in version of Figure 5, concentrating on the main sequence and the giant branch. The position in this diagram of the Be star KIC 6954726, a previously known Be star identified as having infrared excess in the first observation of the KTT, and of BD +20 307, a G0V binary (not in the Kepler field but discussed further below) known from IRAS

[12] See updated table at https://www.pas.rochester.edu/~emamajek/EEM_dwarf_UBVIJHK_colors_Teff.txt.

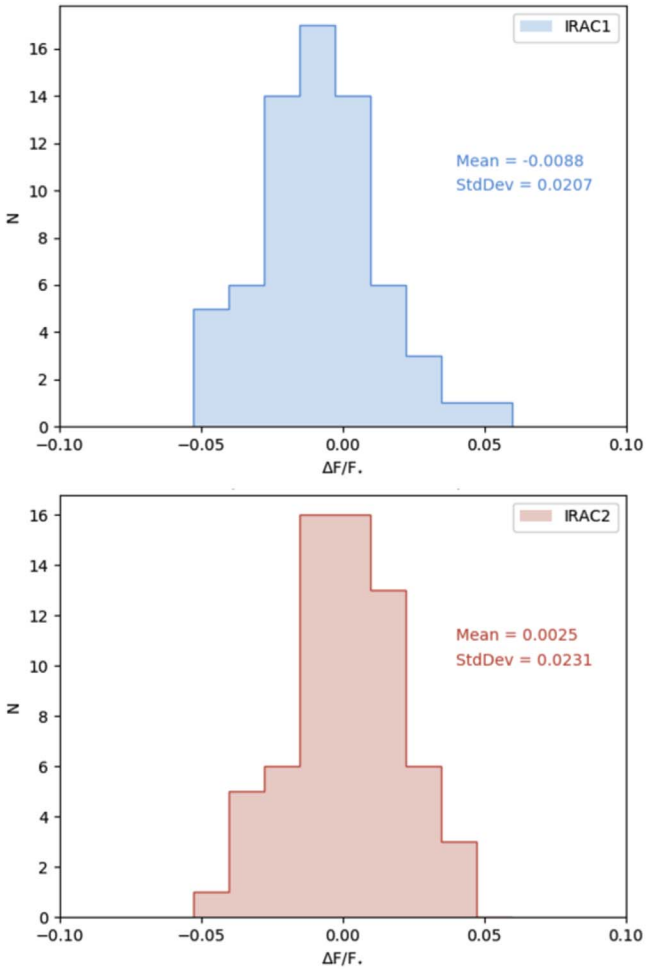

Figure 4. Kepler standard stars confirm the absolute calibration accuracy of the SpiKeS photometry. The histograms show the offset between the model-predicted photosphere flux and the actual IRAC1 (upper panel in blue) and IRAC2 (lower panel in red) measurements, in units of the ratio of the difference in flux to the predicted photosphere value, with a bin size of 0.0125. The 67 Kepler standard stars have a $<3\sigma$ offset, with mean values of -0.0088 in IRAC1 and 0.0025 in IRAC2 and dispersion between 0.02 and 0.023, which reflects the accuracy of the SpiKeS flux measurements and the validity of the Spitzer calibration (see text).

data to have a strong infrared excess (Song et al. 2005), draws our attention to stars lying above the main sequence in this diagram. This is the region of color–color space reached by adding, to a main-sequence star, blackbody emission with a temperature between ∼300 and ∼750 K as might be produced by warm dust or a massive substellar companion. In the hope of finding additional strong excesses, we have examined in detail the SEDs of ∼40 stars that lie in the region above the main locus of stars in Figure 6 and identified two interesting examples: the intrinsically very red star KIC 9655667 and the star KIC 3852667, which appears to have a very strong excess attributable to dust. The fitted SEDs for these stars as well as for the Be star KIC 6954726 are shown in Figure 7, and their properties are summarized in Table 3.

The star KIC 6954726 (StHA 166; $V = 11.76$ mag) in the KTT is a known Be star (Stephenson 1986; Balona et al. 2011) and shows clear evidence for an infrared excess in the SpiKeS data (Figure 7). The WISE photometry for this star is flagged as being possibly contaminated by the nearby bright star HD 184875 (∼100″ separation), so it would have been dropped from the infrared excess search of Kennedy & Wyatt (2012). However, the WISE photometry is in good agreement with SpiKeS. Because this is a known Be star, it is likely that the infrared excess is due to free–free emission, as is seen for other Be stars (Woolf et al. 1970; Dyck & Milkey 1972; Chen et al. 2016).

KIC 3852667 has the strongest infrared excess we have found among stars monitored by Kepler that can be confidently attributed to emission from circumstellar dust. This star, classified as an A supergiant in the KIC, has not been well studied, so the origin of the dust producing the 3.6 and 4.5 μm excess is uncertain. If it is associated with the star rather than with an unseen companion, it has $T_{\rm dust} = 925$ K and is located at a distance of ∼0.5 au from the star with a dust mass of $M_{\rm dust} = 0.75 M_{\rm Moon}$. As shown in Figure 7, this star is detected very solidly in bands 3 and 4 [12 and 22 μm] of the WISE survey. In fact the SED of KIC 3852667 is very similar to that of BD +20 307, which shows a modest excess at 3–5 μm and a much larger excess at 12 and 25 μm (Song et al. 2005). The implications of this similarity are discussed further below.

One of our objectives in carrying out the SpiKeS survey was to search for cool companions—such as brown dwarfs or very late M stars—of main-sequence stars. In this regard, it is possible in principle that the ∼900 K excess reported for KIC 3852267 could be due to such a companion. However, in this case, the star, at a temperature of ∼10,000 K, is so much warmer than the putative companion that the latter would have to be much larger than the star to account for the observed excess radiation. Paradoxically, the best chance for finding a cool companion would be to look for excess emission around an M star, where the ratio of the emission from the companion to that from the star would be highest.

Also shown in Figures 6 and 7 are the colors and fitted spectrum of the star KIC 9655667. This is an M4 dwarf with a temperature of 3100 K. The low temperature and the strong molecular bands in its fitted spectrum (Figure 7) mean that its photospheric colors alone place it in the region of our color–color plot occupied by main-sequence stars with excess emission due to circumstellar dust.

We call attention to BD +20 307 in part because Kennedy & Wyatt (2013) observed that 12 μm excesses as large as that seen in this star, which has $L_{\rm IR}/L_{\rm star} > 0.04$, occur with a frequency of 1 in 10,000 among mature main-sequence stars. As is shown in Figure 6 and can also be seen in data from Song et al. (2005) and Meng et al. (2015), BD +20 307 also shows emission above the stellar photosphere at 3.6 and 4.5 μm. Such excess emission in the short-wavelength IRAC bands occurs only infrequently around mature main-sequence stars; it is gratifying that our color–color plot successfully identifies a star with known excess emission at 3.6 and 4.5 μm. While the 12 μm excess frequency of 1 in 10,000 may be different at 3–5 μm, deriving the frequency at the shorter wavelengths would yield information about the typical dust temperatures in these extreme systems, e.g., a similar detection rate would imply that BD +20 307–like dust distributions are typical for giant impact debris around Sun-like stars (as found tentatively by Wyatt et al. 2017).

Song et al. (2005) argue that the grains responsible for the 3.6 and 4.5 μm emission and those producing the very marked silicate feature responsible for the 12 μm excess will have very short lifetimes around a solar-type star such as BD +20 307. They suggest that the radiating dust is produced by cataclysmic collisions that destroyed an asteroid with a diameter of ∼300 km (see also Meng et al. 2015). It is plausible that the dust around KIC

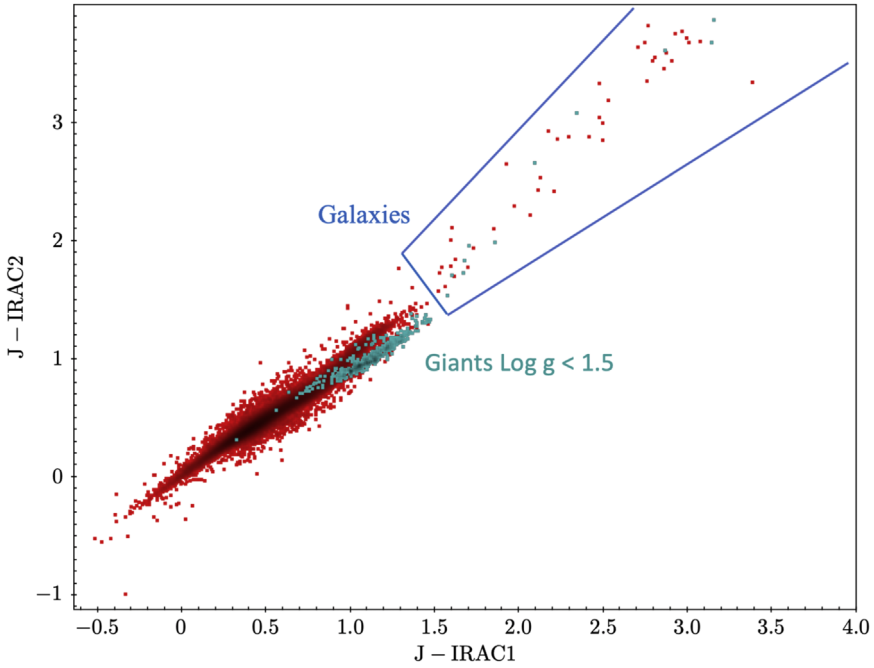

Figure 5. *J*-IRAC1 vs. *J*-IRAC2 for all SpiKeS targets with reliable measurements at both bands. Giants with $\log(g) < 1.5$ based on data in Mathur et al. (2017) are identified as teal points. The region where galaxies have significant representation is noted on the upper right.

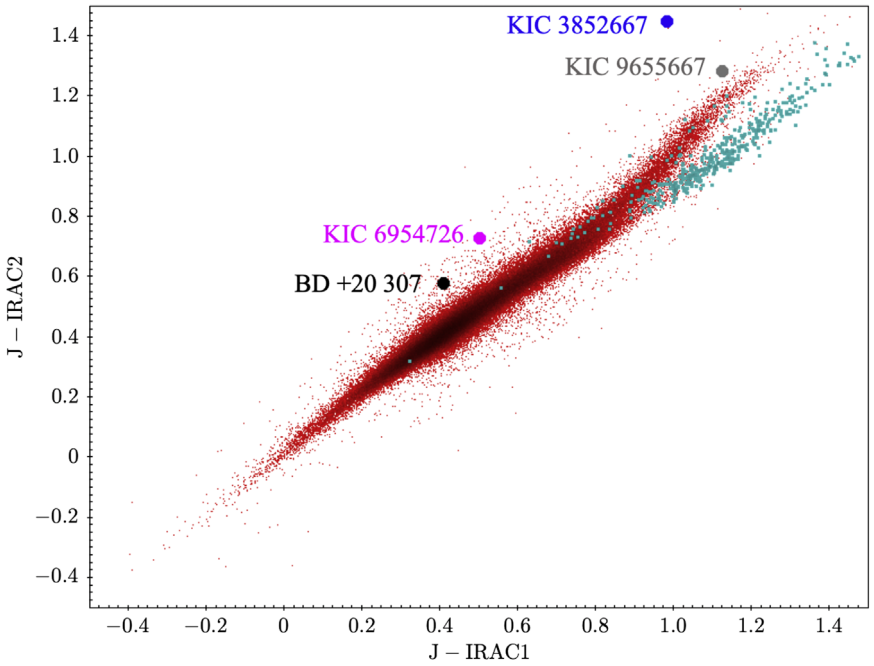

Figure 6. The inner region of the *J*-IRAC1/*J*-IRAC2 color–color plot is shown. Here we highlight the location of the three extreme infrared excess sources from Table 3 as well as of the infrared excess star BD +20 307 (note that it is not in the Kepler FOV) as an illustration of the direction in which main-sequence stars with near-infrared thermal excesses would move in this color space. Teal points are giants selected based on $\log(g) < 1.5$.

3852667, which also shows a pronounced 12 and 25 μm excess, is produced by a similar event. In the future, we will search the SpiKeS data for cases where excess emission as seen by Spitzer at 3.6 and 4.5 μm is accompanied by strong emission in the WISE 12 μm band; these could be further instances of this scenario.

In looking for infrared excesses, we also consider planet-host stars targeted in the Robo-AO Kepler Planetary Candidate Survey (Ziegler et al. 2017). We consider planet-host stars that have been observed by Robo-AO and shown to not have companions between 0.″5 and 4.″0, thus raising the likelihood that a detected excess would be from dust and not from a companion. We performed a detailed SED analysis (as described in Section 3.4) on 252 out of 332 of these stars, for which updated stellar parameters are known from the references listed in Section 3.4 and which are detected below the IRAC1 and IRAC2 saturation levels. We found all SEDs for this sample of stars to be photospheric in the IRAC wave bands to within 10%.

We caution the reader that a star lying in the region above the main sequence (Figure 6) has to be examined in detail

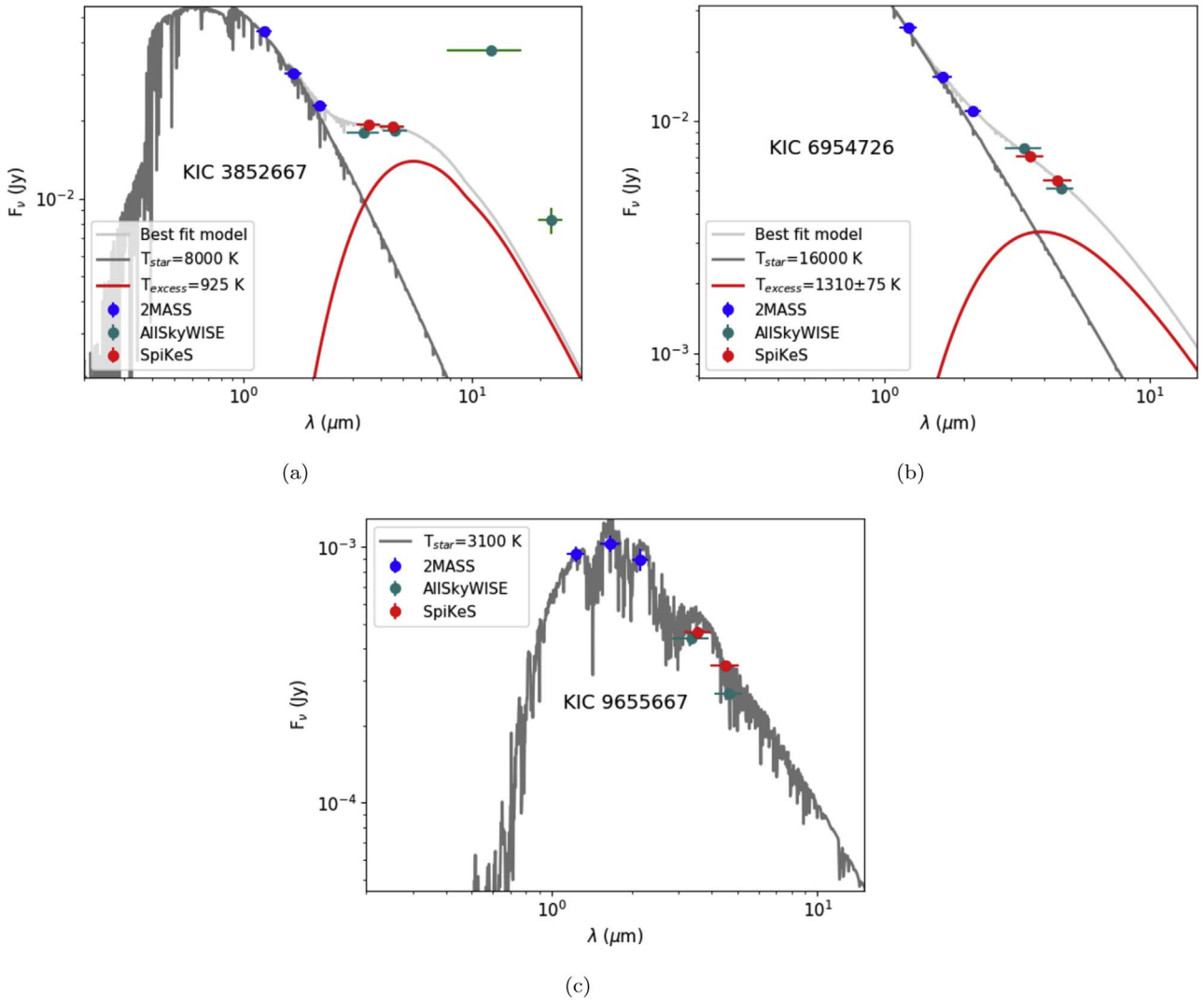

Figure 7. SED fits to a selection of sources that are above the main locus of points in Figure 6. (a) KIC 3852667 is an example of warm dust around an A-type supergiant star. (b) KIC 6954726 is the previously identified Be star. (c) KIC 9655667 is a cool red M-type star.

Table 3
Properties of Stars Shown with SEDs in Figure 6

KIC #	Other ID	Sp. Type	Dist. (pc)	N_{obs}	$F_{excess,I1}/F_\star$	$F_{excess,I2}/F_\star$
3852667	TYC 3134-254-1	A0Ib	15,160	3	1.16	2.26
6954726	EM* StHA 166	B2.5Ve	4170	3	0.92	1.37
9655667	2MASS J19374305 + 4621555	M4	290	4	...	...

before any conclusions can be drawn about a possible infrared excess. This is illustrated by the red star KIC 965567, discussed earlier, which lies in this region based on its photospheric colors alone (see Figures 6 and 7). Note also that many candidate infrared excess sources identified by their location in the *J*-IRAC1 versus *J*-IRAC2 figure proved to have close companions in the Spitzer images. Although the main target in those closely spaced sources may indeed have an infrared excess, we cannot without further work rule out contamination by the close companion. We have also found that image artifacts that have slipped through our vetting process can, albeit infrequently, mimic infrared excesses. Finally, contamination due to a background galaxy is another possible source of false positives in a search for infrared excesses.

5. Summary and Conclusions

We have presented a new catalog of Spitzer 3.6 μm (IRAC1) and 4.5 μm (IRAC2) infrared photometry of nearly all the stars monitored by Kepler during its 4 yr prime mission. By applying corrections at the individual exposure level we have achieved a photometric precision better than the nominal Spitzer calibration uncertainty of 2.4%. For the purposes of comparison between sources within this survey, the uncertainties are 1.2% to 2.3%, depending on the brightness of the sources. These uncertainties are derived from a comparison of more than 10,000 sources in a KTT that was observed in two epochs and allowed for an estimation of the systematic effects in the data. In all, we report photometry of almost 170,000 sources in both IRAC bands.

We have shown that the SpiKeS data can be fit with very high accuracy by stellar models. This has allowed us to verify independently the claimed 2.4% accuracy of the Spitzer calibration. We have shown a few examples of stars with infrared excesses, but further work is needed to identify robustly the population of stars with excesses or to test whether the finding of Kennedy & Wyatt (2012) that 1 in 10,000 main-sequence stars host bright mid-infrared excesses also applies to near-infrared excesses. In total, we have fit models to SpiKeS and other data for 360 Kepler targets, 67 Kepler standard stars, 41 stars that lie in the region above the main locus of stars in Figure 6, and 252 planet-host stars targeted in the Robo-AO Kepler Planetary Candidate Survey and claim infrared excesses of $\gtrsim$10% in only two, one of which is a previously known Be star. The other is an A0 supergiant.

We have compared our measurements to those from WISE (see Appendix E). Spitzer's higher resolution has allowed us to separate out sources whose fluxes were combined in the lower-resolution WISE beam. We estimate that the Spitzer photometry will be more reliable than that from WISE for ∼2% (∼4000) of the sources seen by both missions; WISE sources suspected to be contaminated in this fashion are flagged in the catalog accompanying this work. Ultimately, precise SED fitting of the SpiKeS and other data, combined with distances measured by Gaia, may lead to improved estimates of the radii of exoplanet host stars and of the radii of transiting exoplanets.

The final reduced data can be accessed from the NASA Exoplanet Archive (NASA-EA),[13] and it will contain both our final photometry and other data for each Kepler target from Mathur et al. (2017), WISE, 2MASS, NASA-EA, and Gaia (Table 4). This will allow us and others to pursue further investigation into lower-level infrared excesses and stellar and exoplanetary properties.

We thank Sean Carey of the SSC for extensive discussions of the systematic effects in the IRAC data and Bob Benjamin for introducing us to red clump giants. We also thank Erik Petigura for discussions of the applicability of the work of Fulton & Petigura (2018) to the SpiKeS data. We thank the anonymous referee for very helpful comments and suggestions which improved the paper. We thank Justin Beaurone for assistance with producing Table 3. We also thank the ever-helpful staff of the SSC for helping us to develop the protocols under which the AORs for each tile of the complete survey could be submitted.

G.M.K. is supported by the Royal Society as a Royal Society University Research Fellow.

The research was carried out at the Jet Propulsion Laboratory, California Institute of Technology (JPL/Caltech), under a contract with the National Aeronautics and Space Administration (80NM0018D0004). This work is based in part on observations made with the Spitzer Space Telescope, which was operated by JPL/Caltech, under a contract with NASA. Support for this work was provided by NASA through an award issued by JPL/Caltech. This publication also makes use of data products from WISE, which is a joint project of the University of California, Los Angeles, and JPL/Caltech, funded by NASA. This work has made use of data from the European Space Agency mission Gaia (https://www.cosmos.esa.int/gaia), processed by the Gaia Data Processing and

[13] The final data will be available at NASA-EA after 2021 April at the following URL: https://exoplanetarchive.ipac.caltech.edu/docs/spikes.html.

Table 4
SpiKeS Table Columns

Column Header	Description
Kepid (KIC)	KepID (KIC number)
KOI (NASA-EA)	Kepler object of interest number
Kepler Name (NASA-EA)	Kepler planet name
R.A. (KIC)	R.A. J2000
Decl. (KIC)	Decl. J2000
I1 flux (SpiKeS)	IRAC1 flux density (mJy)
I1 unc (SpiKeS)	IRAC1 uncertainty (mJy)
I1 mag (SpiKeS)	IRAC1 magnitude
I1 mag unc (SpiKeS)	IRAC1 magnitude uncertainty
I1 n obs (SpiKeS)	IRAC1 number of observations
I2 flux (SpiKeS)	IRAC2 flux density (mJy)
I2 unc (SpiKeS)	IRAC2 uncertainty (mJy)
I2 mag (SpiKeS)	IRAC2 magnitude
I2 mag unc (SpiKeS)	IRAC2 magnitude uncertainty
I2 n obs (SpiKeS)	IRAC2 number of observations
SpiKeS Flags (SpiKeS)	Flags from SpiKeS
kepmag (KIC)	Kepler-band magnitude
kmag err (KIC)	Kepler magnitude uncertainty
tm designation (2MASS)	2MASS designation
jmag (2MASS)	*J*-band magnitude
jmag err (2MASS)	*J*-band error
hmag (2MASS)	*H*-band magnitude
hmag err (2MASS)	*H*-band error
kmag (2MASS)	$K_{\rm short}$-band magnitude
kmag err (2MASS)	$K_{\rm short}$-band error
ALLWISE	WISE All-sky Release Catalog name
RAJ2000 (AllWISE)	R.A. J2000 (deg)
DEJ2000 (AllWISE)	Decl. J2000 (deg)
W1mag (AllWISE)	W1 magnitude
W2mag (AllWISE)	W2 magnitude
W3mag (AllWISE)	W3 magnitude
W4mag (AllWISE)	W4 magnitude
e W1mag (AllWISE)	Mean W1 magnitude error
e W2mag (AllWISE)	Mean W2 magnitude error
e W3mag (AllWISE)	Mean W3 magnitude error
e W4mag (AllWISE)	Mean W4 magnitude error
ID (AllWISE)	Unique WISE source ID
cc flags (AllWISE)	Contamination and confusion flag
ext flg (AllWISE)	Extended source flag
var flg (AllWISE)	Variability flag
qph (AllWISE)	Photometric quality flag
angDist (AllWISE)	Angular separation from SpiKeS source (arcsec)
CatWISE	CatWISE Release Catalog name
RAJ2000 (CatWISE)	R.A. J2000 (deg)
DEJ2000 (CatWISE)	Decl. J2000 (deg)
W1mag (CatWISE)	W1 magnitude
W2mag (CatWISE)	W2 magnitude
e W1mag (CatWISE)	Mean W1 magnitude error
e W2mag (CatWISE)	Mean W2 magnitude error
teff (Mathur et al.)	Stellar effective temperature (K)
teff err1 (Mathur et al.)	Temperature error + (K)
teff err2 (Mathur et al.)	Temperature error − (K)
logg (Mathur et al.)	Stellar surface gravity [$\log_{10}$(cm*s^{-2})]
logg err1 (Mathur et al.)	log(g) error +
logg err2 (Mathur et al.)	log(g) error −
feh (Mathur et al.)	Stellar metallicity
feh err1 (Mathur et al.)	FeH error +
feh err2 (Mathur et al.)	FeH error −
mass (Mathur et al.)	Stellar mass (solar masses)
mass err1 (Mathur et al.)	Mass error +
mass err2 (Mathur et al.)	Mass error −
radius (Mathur et al.)	Stellar radius (solar radii)
radius err1 (Mathur et al.)	Stellar radius error +
radius err2 (Mathur et al.)	Stellar radius error −

Table 4
(Continued)

Column Header	Description
dens (Mathur et al.)	Stellar density (g cm^{-3})
dens err1 (Mathur et al.)	Stellar density error +
dens err2 (Mathur et al.)	Stellar density error −
av (Mathur et al.)	A_v extinction (mag)
av err1 (Mathur et al.)	A_v error +
av err2 (Mathur et al.)	A_v error −
Gaia id	Unique Gaia identifier
RA ICRS (Gaia)	Barycentric R.A. J2015.5
DE ICRS (Gaia)	Barycentric decl. J2015.5
rest (Gaia)	Bailer-Jones+ 2018 estimated distance (pc)
b rest (Gaia)	Lower bound on the confidence interval of the estimated distance (pc)
B rest (Gaia)	Upper bound on the confidence interval of the estimated distance (pc)
rlen (Gaia)	Length scale used in the prior for the distance estimation (pc)
ResFlag (Gaia)	Result flag
ModFlag (Gaia)	Number of modes in the posterior
parallax (Gaia)	Absolute stellar parallax (mas)
parallax error (Gaia)	Standard error of parallax (mas)
pmra (Gaia)	Proper motion in R.A. direction (mas yr^{-1})
pmra error (Gaia)	Standard error of proper motion in R.A. direction (mas yr^{-1})
pmdec (Gaia)	Proper motion in decl. direction (mas yr^{-1})
pmdec error (Gaia)	Standard error of proper motion in decl. direction (mas yr^{-1})
angDist (Gaia)	Angular separation from SpiKeS sources (arcsec)

Analysis Consortium (DPAC, https://www.cosmos.esa.int/web/gaia/dpac/consortium). Funding for the DPAC has been provided by national institutions, in particular the institutions participating in the Gaia Multilateral Agreement.

Software: Astropy (Astropy Collaboration et al. 2013, 2018), TOPCAT (Taylor 2005), SExtractor (Bertin & Arnouts 1996).

Appendix A
Photometric Corrections

A.1. Systematic Effects

Because we were hoping to do ∼1% photometry on stars as bright as 10th mag, we had to deal with several systematic effects that do not materially influence Spitzer photometry of faint objects but become important for bright stars that could be photon noise–limited with an uncertainty considerably less than 1%.

1. Intrapixel sensitivity variations (the pixel phase effect). The signal received from a star can vary by as much as ∼8% and ∼3% for IRAC1 and IRAC2, respectively, depending on where the centroid of the stellar image falls in the $1\farcs2 \times 1\farcs2$ pixel. This variation is due to intrapixel spatial variations in effective quantum efficiency. For the pixel phase effect, the centroid of the image on the array is determined by the SSC software box_centroid.pro. The SSC provides an IDL routine (pixel_phase_correct_-gauss.pro) for correcting this effect as a function of location on the pixel, which is an average over the array, but does not tabulate such a routine separately for each of the 65,000+ pixels in each IRAC array. We use this average correction in our analysis.
2. Array location–dependent photometric corrections for compact sources with stellar spectral slopes. This correction is required to compensate for the fact that IRAC is flat-fielded using the zodiacal background, which is not valid for compact sources with starlike SEDs. It also responds to the fact that the filter effective wavelength varies across the array. This effect can change the inferred flux by 1.3% on average, with the effect increasing to ∼5% for stars at the edge of the array in IRAC1 and to ∼8% in IRAC2. The correction consists of 2D arrays provided by the SSC in FITS format. This correction also removes the photometric effect of the spatial distortions across the IRAC arrays.

A.2. Outlier Rejection

For individual photometric measurements on each CBCD image, we used the 2 pixel radius, which is the smallest photometry aperture that has aperture corrections determined for it by the SSC. This was done to have the least impact by bad pixels and cosmic-ray hits within the photometry aperture. Any image that had a bad pixel from the bad pixel mask (generated by the SSC's pipeline) within the 2 pixel radius aperture was eliminated in keeping with our efforts to have a high-reliability catalog: data from the star in question were not reported for that CBCD. This was done before the medianing process and so sometimes reduced the number of observations from the planned three visits from the survey strategy. See Appendix B for the final numbers.

Another set of outliers were discovered when comparing our data to 2MASS data (in this case K_s-IRAC1 versus K_s-IRAC2). These sources had near zero color on one color axis but extreme color on the other axis. A similar effect was seen when the WISE data were compared to the SpiKeS data. For a given star, the IRAC1–WISE1 flux ratio would be close to zero, while IRAC2–WISE2 indicated a major discrepancy between the two missions, or vice versa.

After examination of the images for these outliers we have found that these sources are affected by nearby very bright sources in one channel. This artifact, a column pull-up that remains on the array after a very bright source has been observed at that location, was previously identified by the SSC but is rare and is not corrected for in the pipeline processing like other artifacts.[14] Note that a column pull-down effect also exists, which is corrected for in the SSC pipeline processing.

So to have a final catalog of high-quality photometric measurements, we have decided to exclude the photometry for the affected channel. We have accomplished this by excluding the IRAC2 datum for cases where the WISE1–IRAC1 color is near zero and the WISE2–IRAC2 color is significantly (5σ from the mean) displaced from zero, and by excluding the IRAC1 datum when the WISE2–IRAC2 color is near zero but the WISE1–IRAC1 color is 5σ from the mean.

The net result of the outlier rejection is a final catalog with 174,667 sources measured at IRAC1, 179,896 measured at IRAC2, and 169,828 sources with both IRAC1 and IRAC2 photometry.

[14] See Sections 5.2.4 and 7.2.4 in the IRAC Instrument Handbook: https://irsa.ipac.caltech.edu/data/SPITZER/docs/irac/iracinstrumenthandbook/.

Appendix B
Summary of the Number of Usable Measurements per Kepler Target at Each of the Two IRAC Bands for the Full Survey [PID 10067]

Table B1 contains a summary of the number of times each source was measured in each of the two IRAC bands for the full survey. As per the design of the survey, the majority in each band have three measurements.

Table B1
Number of Usable Measurements per Kepler Target

Number of Measurements	IRAC1 Number/Percent	IRAC2 Number/Percent
0	17,317/9%	12,088/6%
1	13,843/7%	15,915/8%
2	29,665/15%	38,015/20%
3	104,051/54%	103,172/54%
4	20,916/11%	18,429/10%
5	3282/2%	2780/1%
6	2455/1%	1349/<1%
7–10	455/<1%	236/<1%
Total	191,984/100%	191,984/100%

Appendix C
Journal of Observations for PID 10067

Table C1 presents the log of the Spitzer observations for the main survey spanning from 2013 December to 2015 January. The Kepler Test Tile was observed in 2013 January.

Table C1
Journal of Observations for PID 10067

Name	Center R.A. J2000	Center Decl. J2000	Observation Start–End UT
Tile 2	281.912740	43.439774	2013-12-21 01:30:43–2013-12-22 08:24:31
Tile 3	284.289690	41.200925	2013-12-22 19:24:15–2013-12-24 01:12:53
Tile 4	286.506490	38.917202	2014-11-28 01:15:00–2014-11-29 04:06:54
Tile 6	282.519590	47.459067	2013-12-25 01:47:33–2013-12-26 07:05:40
Tile 7	285.054680	45.201847	2013-12-27 03:24:25–2013-12-28 09:07:08
Tile 8	287.391890	42.892913	2014-12-04 23:36:35–2014-12-06 00:56:16
Tile 9	289.562980	40.539820	2013-12-28 17:06:02–2013-12-29 23:12:19
Tile 10	291.582260	38.151037	2013-12-29 23:13:46–2013-12-31 07:06:55
Tile 11	285.905820	49.198153	2013-12-31 07:55:48–2014-01-01 14:36:05
Tile 12	288.390390	46.873261	2014-12-07 20:08:11–2014-12-08 23:41:58
Tile 13	290.667160	44.496534	2014-01-02 22:13:18–2014-01-04 04:09:00
Tile 14[a]	292.765220	42.080201	2014-01-04 04:19:27–2014-01-05 16:27:09
Tile 15	294.707160	39.626466	2014-01-05 20:15:49–2014-01-07 01:20:16
Tile 16	289.529890	50.834433	2014-12-20 13:34:58–2014-12-21 18:42:55
Tile 17	291.935230	48.441523	2014-10-04 00:05:30–2014-10-05 05:05:15
Tile 18	294.121620	46.002749	2014-10-06 21:29:23–2014-10-08 05:24:24
Tile 19	296.123050	43.525787	2014-12-26 08:38:46–2014-12-27 13:50:44
Tile 20	297.966030	41.015652	2015-01-05 18:02:54–2015-01-06 22:49:08
Tile 22	295.693870	49.894773	2015-01-30 17:19:11–2015-01-31 23:30:47
Tile 23	297.760040	47.397734	2015-01-11 12:01:32–2015-01-12 17:48:36
Tile 24	299.639180	44.868238	2015-01-17 17:25:00–2015-01-18 15:14:27

Note.
[a] The PID 90100 observations of Tile 14 took place on 2013 January 9 02:42:50–23:33:02.

Appendix D
Stellar Variability

The consistency of the photometry allows us to make statements about the inherent infrared variability of the ∼11,000 sources monitored by Kepler in the KTT and then extend that to the expected variation over all Kepler tiles.

We took the difference between the epoch 1 and epoch 2 flux measurements between 9th and 14th mag, and there were 131 (1.2%) IRAC1 sources and 112 (1.1%) IRAC2 sources that had a 3σ or greater difference between the two epochs. Our expectation is that any physically real variability would have affected both the IRAC1 and IRAC2 channels in a similar direction. Of the sources that varied, only 23 (0.2%) had the same sign for their difference where both channels got fainter or both channels got brighter between the two epochs. Based on this result from the KTT then, over all the 21 Kepler tiles, only about ∼400 sources would have varied at the 3σ level over one year's time. This sets a conservative upper limit of <1% for sources affected by variability that changed their flux by more than 3σ. This small number is likely a result of primarily choosing stable main-sequence stars as the bulk of the sources for Kepler to monitor.

Appendix E
Comparison with WISE

The WISE mission surveyed the entire sky at wavelengths of 3.4, 4.6, 12, and 22 μm (known as bands WISE1–4). WISE1 and WISE2 are very similar to IRAC bands 1 and 2, so here we compare our SpiKeS photometry to the WISE photometery, drawing in part on the study by Kennedy & Wyatt (2012) of the WISE measurements of the Kepler field. This comparison illuminates some important features of the SpiKeS data. WISE has a 40 cm telescope and 3.4 and 4.6 μm arrays with 1024 pixels, with an FOV of 47′. The pixel size is 2.″5, and the beam size is 6″. WISE scans continuously, using a step-and-stare strategy incorporating a scan mirror in the focal plane to freeze each FOV on the sky for ∼11 s before jumping ahead to the next. Eight or more independent exposures were obtained at each point in the sky during the 6 month prime mission. Like Spitzer, WISE continued to operate at its two shortest bands even after cryogen depletion, first as the Near Earth Object WISE (NEOWISE) survey (Mainzer et al. 2011) and then as the NEOWISE Reactivation (NEOWISE-R) survey (Mainzer et al. 2014), both collecting data in the same fashion as the original mission. The WISE data described here come from the AllWISE catalog compiled from the first two years of the mission as a part of the WISE and NEOWISE mission phases, which includes four separate epochs of measurement of each star following the protocol above. Matching with the Spitzer data was done using the best match within 1″ between the two catalogs. Since there are cases where there are two Spitzer sources within the WISE beam (see Appendix E.1), the match in the SpiKeS catalog is the Spitzer source closest to the location assigned to the WISE source. Kennedy & Wyatt (2012) matched the AllWISE catalog to the Kepler catalog and showed that there were ∼130 K reliable sources (defined as those having no cautionary flags set) at WISE1 and WISE2, while the SpiKeS matches to the Kepler catalog yielded almost ∼170 K reliable sources at IRAC1 and IRAC2. While the additional measurements available from CatWISE2020 (see below) should increase the number of reliable detections in WISE1 and WISE2, we anticipate that there will be many sources, beyond the 4000 described below, for which WISE does not provide reliable detections while SpiKeS does.

Near the time of this paper's submission a new WISE catalog named CatWISE2020 was released combining data from the WISE, NEOWISE, and NEOWISE-R surveys (Marocco et al. 2021), spanning observations from 2010 January to 2018 December. Because we use the WISE data quantitatively only for outlier rejection (Appendix A.2) and because the CatWISE2020 catalog fluxes agree well with the AllWISE catalog, we continue to use the data from the AllWISE catalog for comparisons with SpiKeS results. The larger number of observations in the CatWISE2020 catalog allows for an assessment of variability for the SpiKeS sources. Our assessment of the variability of sources based on the CatWISE2020 catalog's variability flags is consistent with our assessment that less than 1% of the sources are variable as also discussed in Appendix D.

Before comparing the AllWISE and SpiKeS data on the Kepler field, we should emphasize that overall the two surveys agree very well on the brightness of individual stars. This is shown by Figure 8, which compares the SpiKeS and AllWISE

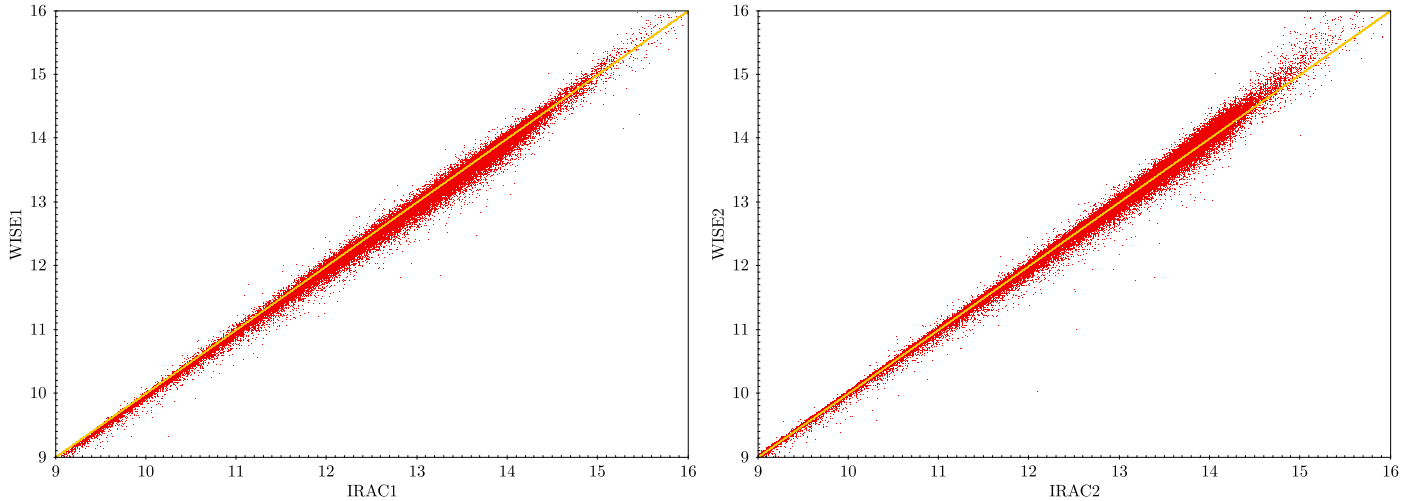

Figure 8. Comparison of AllWISE photometry to Spitzer photometry for dwarf stars ($\log(g) > 4$). Left: IRAC1 vs. WISE1. Right: IRAC2 vs. WISE2. The diagonal line is $x = y$. The slope and offset trends reproduce those in the original Spitzer and WISE comparison in Jarrett et al. (2011).

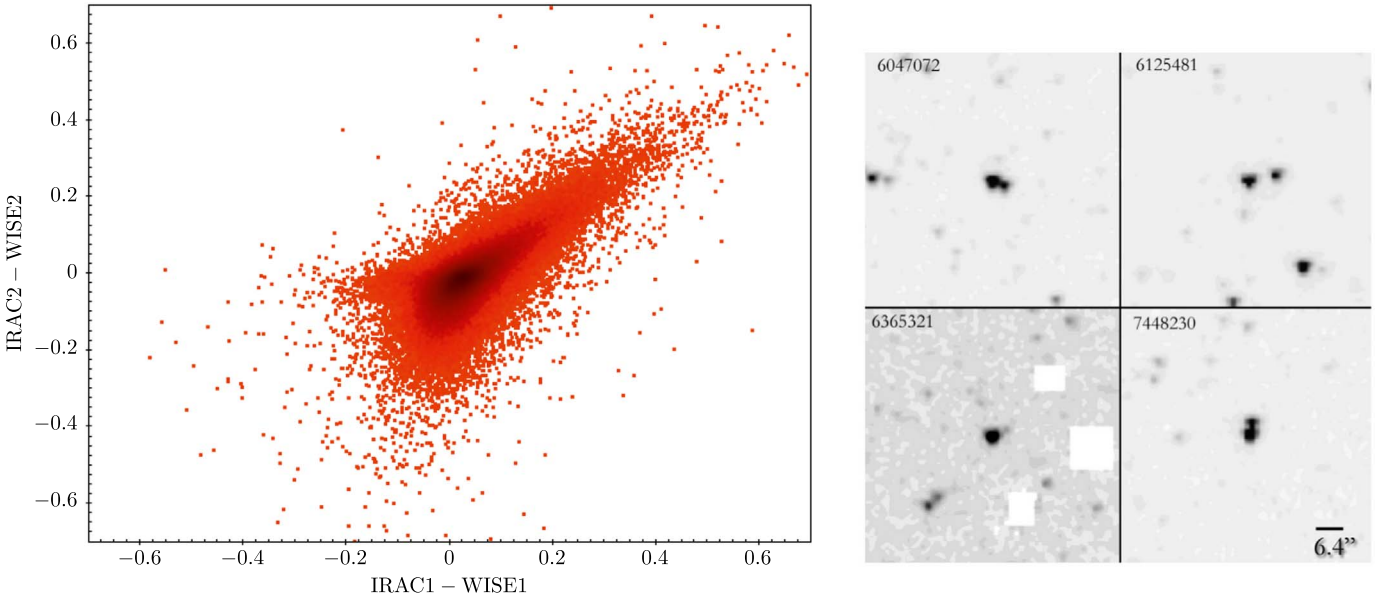

Figure 9. Left: Brightness comparison of WISE and SpiKeS observations for all available Kepler targets in the KTT showing that there is a population of sources that have WISE fluxes brighter than the Spitzer fluxes, leading to a spur of sources to the upper right away from zero–zero. Right: Upon individual examination most of these sources turn out to be double sources in the higher-resolution Spitzer images. Spitzer has 10× better areal resolution with a 1.″6 FWHM image vs. the WISE 6′ image.

photometry for stars classified as dwarfs by Mathur et al. (2017) ($\log(g) > 4$). The line is simply $x = y$, not a fit to the data. Overall, our comparison of Spitzer and AllWISE photometry is consistent with the results of a more extensive comparison at the North Ecliptic Pole between the two missions by Jarrett et al. (2011).

E.1. Spatial Resolution

A major advance of Spitzer over WISE for the study of the Kepler stars comes from improvements in spatial resolution. This is illustrated qualitatively in Figure 9, which compares the WISE and SpiKeS fluxes for the two epochs of the KTT. The spur to the upper right from the central concentration is produced by stars that appear brighter as seen by WISE than as seen by Spitzer. This is the signature of a contaminating source in the large WISE beam, as is illustrated by Spitzer images of a handful of these overbright objects. From the data shown in Figure 9, we estimate that at least ∼2% (∼4000) of the WISE sources are double or multiple. Such contamination is reduced in the data of Spitzer because of its smaller beam size of 1.″8–2″ versus the WISE beam size of 6″.

E.2. Senstivity Comparison

Like Spitzer, WISE will be stellar photon noise–limited for observations of the brightest stars. Spitzer's precision for such stars is dominated by systematic effects amplified by the fact that most stars are sampled only one to four times. In the stellar photon noise limit, the two surveys should have comparable sensitivity, with Spitzer's larger aperture being balanced out by WISE's longer integration time. In addition, AllWISE, with a typical eight samples/epoch, four separate epochs of observation, and a considerably oversampled image, should suffer smaller systematic effects. Hence the reported precision of AllWISE could exceed that of Spitzer for the brightest stars. In fact, we found that AllWISE is somewhat more precise than Spitzer for stars brighter than about 12th mag. Spitzer becomes more precise at about 13th mag. Beyond 14th mag Spitzer is significantly more precise than AllWISE. With the additional data of CatWISE2020, the sensitivity advantage of WISE over Spitzer may extend to fainter magnitudes.

Appendix F
Using Gaia Distances to Determine an HR Diagram

With the release of Gaia DR2 a larger and more accurate database of distances has become available for the Kepler targets. We have matched the Gaia sources using the same approach we used for matching to the WISE sources, where a 1″ radius was used to associate a Spitzer source with a Gaia source. The difference here is that Gaia has higher resolution than Spitzer, and so, if there was more than one Gaia source within the Spitzer beam, then the Gaia source closest to the Spitzer source's location would be associated in the SpiKeS catalog. Using the distances derived from Gaia by Bailer-Jones et al. (2018) we have determined absolute magnitudes for our SpiKeS sources and have plotted them in Figure 10. This infrared HR diagram is very similar to the optical HR diagram of Kepler stars derived by Berger et al. (2020). The main parts of the HR diagram are clearly distinguishable: the main sequence, the red giant branch, the asymptotic giant branch, and the red giant clump. The main-sequence region seems to have two distinct concentrations: a main, highly dense one and a more luminous but less dense one above it in the cooler region of the main sequence (*J*-IRAC1 of 0.6–1.0). This was also noted in Berger et al. (2020), and they labeled these sources as cool main-sequence binaries. These are binary stars that are unresolved by Gaia (and also Spitzer) and so have a single distance associated with a point source that has a flux composed of two stars; thus its absolute magnitude is higher than would be expected from its color.

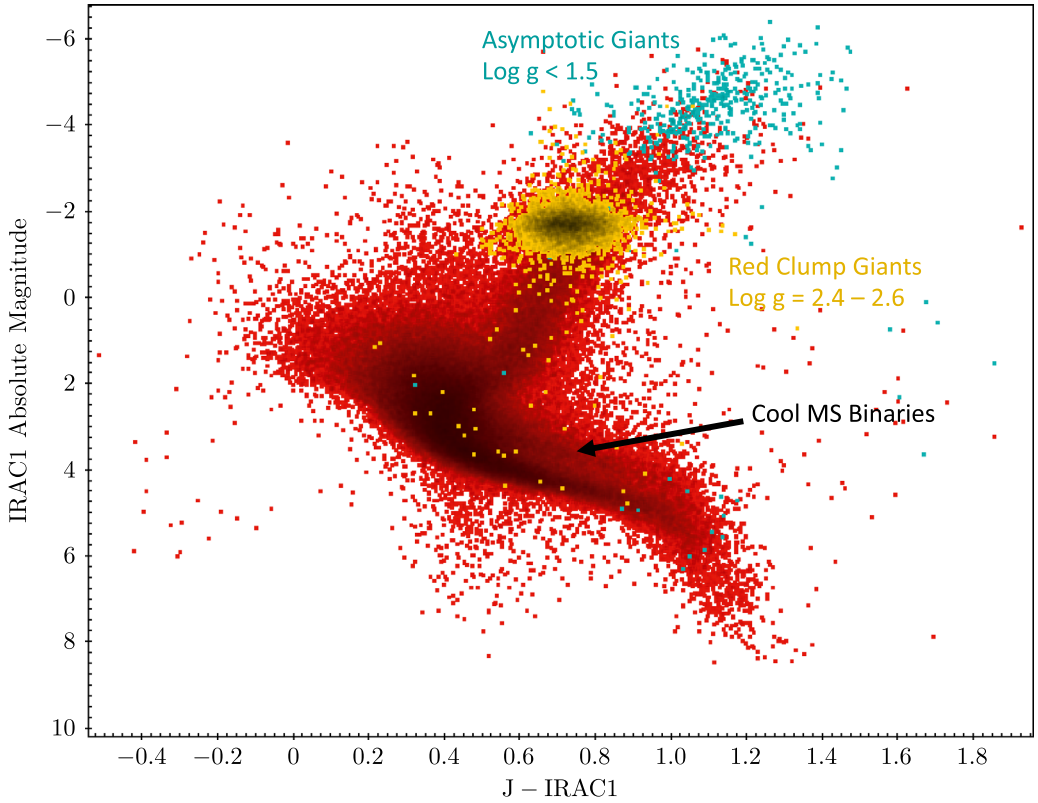

Figure 10. Using distances from Gaia DR2 we have generated an HR diagram of our SpiKeS sources. The main sequence, the giant branch, the red clump giants, and the asymptotic giant branch are clearly identifiable. The asymptotic giants and the red clump giants are also distinguished based on their log(g). Also there is a concentration of sources right above the main sequence, which are unresolved cool main-sequence binaries.

ORCID iDs

Michael W. Werner https://orcid.org/0000-0003-4990-189X
Varoujan Gorjian https://orcid.org/0000-0002-8990-2101
Farisa Y. Morales https://orcid.org/0000-0001-9414-3851
John H. Livingston https://orcid.org/0000-0002-4881-3620
Grant M. Kennedy https://orcid.org/0000-0001-6831-7547
Rachel L. Akeson https://orcid.org/0000-0001-9674-1564
Charles Beichman https://orcid.org/0000-0002-5627-5471
David R. Ciardi https://orcid.org/0000-0002-5741-3047
Elise Furlan https://orcid.org/0000-0001-9800-6248
Patrick J. Lowrance https://orcid.org/0000-0001-8014-0270
Eric E. Mamajek https://orcid.org/0000-0003-2008-1488
Peter Plavchan https://orcid.org/0000-0002-8864-1667
Mark C. Wyatt https://orcid.org/0000-0001-9064-5598

References

Astropy Collaboration, Price-Whelan, A. M., Sipőcz, B. M., et al. 2018, AJ, 156, 123
Astropy Collaboration, Robitaille, T. P., Tollerud, E. J., et al. 2013, A&A, 558, A33
Bailer-Jones, C. A. L., Rybizki, J., Fouesneau, M., Mantelet, G., & Andrae, R. 2018, AJ, 156, 58
Balona, L. A., Pigulski, A., De Cat, P., et al. 2011, MNRAS, 413, 2403
Berger, T. A., Huber, D., van Saders, J. L., et al. 2020, AJ, 159, 280
Bertin, E., & Arnouts, S. 1996, A&AS, 117, 393
Bohlin, R. C., Gordon, K. D., Rieke, G. H., et al. 2011, AJ, 141, 173
Borucki, W. J., Koch, D., Basri, G., et al. 2010, Sci, 327, 977
Boyajian, T. S., LaCourse, D. M., Rappaport, S. A., et al. 2016, MNRAS, 457, 3988
Carey, S., Ingalls, J., Hora, J., et al. 2012, Proc. SPIE, 8442, 84421Z
Chaplin, W. J., Basu, S., Huber, D., et al. 2014, ApJS, 210, 1
Chaplin, W. J., Kjeldsen, H., Bedding, T. R., et al. 2011, ApJ, 732, 54
Chen, C. H., Mittal, T., Kuchner, M., et al. 2014, ApJS, 211, 25
Chen, P. S., Liu, J. Y., & Shan, H. G. 2016, MNRAS, 463, 1162
Ciardi, D. R., von Braun, K., Bryden, G., et al. 2011, AJ, 141, 108
Draine, B. T. 2003, ARA&A, 41, 241
Dyck, H. M., & Milkey, R. W. 1972, PASP, 84, 597
Fazio, G. G., Hora, J. L., Allen, L. E., et al. 2004, ApJS, 154, 10
Fulton, B. J., & Petigura, E. A. 2018, AJ, 156, 264
Gaia Collaboration, Brown, A. G. A., Vallenari, A., et al. 2018, A&A, 616, A1
Gaia Collaboration, Prusti, T., de Bruijne, J. H. J., et al. 2016, A&A, 595, A1
Huber, D., Bedding, T. R., Stello, D., et al. 2011, ApJ, 743, 143
Jarrett, T. H., Cohen, M., Masci, F., et al. 2011, ApJ, 735, 112
Kennedy, G. M., & Wyatt, M. C. 2012, MNRAS, 426, 91
Kennedy, G. M., & Wyatt, M. C. 2013, MNRAS, 433, 2334
Li, J., Smith, M. C., Zhong, J., et al. 2016, ApJ, 823, 59
Mainzer, A., Bauer, J., Cutri, R. M., et al. 2014, ApJ, 792, 30
Mainzer, A., Bauer, J., Grav, T., et al. 2011, ApJ, 731, 53
Marengo, M., Hulsebus, A., & Willis, S. 2015, ApJL, 814, L15
Marocco, F., Eisenhardt, P. R. M., Fowler, J. W., et al. 2021, ApJS, 253, 8
Mathur, S., Huber, D., Batalha, N. M., et al. 2017, ApJS, 229, 30
Meng, H. Y. A., Su, K. Y. L., Rieke, G. H., et al. 2015, ApJ, 805, 77
Mushotzky, R. F., Edelson, R., Baumgartner, W., & Gandhi, P. 2011, ApJL, 743, L12
Pecaut, M. J., & Mamajek, E. E. 2013, ApJS, 208, 9
Petigura, E. A., Howard, A. W., Marcy, G. W., et al. 2017, AJ, 154, 107
Rieke, G. H., & Lebofsky, M. J. 1985, ApJ, 288, 618
Skrutskie, M. F., Beichman, C., Capps, R., et al. 1995, AAS Meeting, 187, 75.07
Song, I., Zuckerman, B., Weinberger, A. J., & Becklin, E. E. 2005, Natur, 436, 363
Stephenson, C. B. 1986, ApJ, 300, 779
Taylor, M. B. 2005, in ASP Conf. Ser. 347, Astronomical Data Analysis Software and Systems XIV, ed. P. Shopbell, M. Britton, & R. Ebert (San Francisco, CA: ASP), 29
Verner, G. A., Elsworth, Y., Chaplin, W. J., et al. 2011, MNRAS, 415, 3539
Werner, M. W., Roellig, T. L., Low, F. J., et al. 2004, ApJS, 154, 1
Woolf, N. J., Stein, W. A., & Strittmatter, P. A. 1970, A&A, 9, 252
Wright, E. L., Eisenhardt, P. R. M., Mainzer, A. K., et al. 2010, AJ, 140, 1868
Wyatt, M. C., Bonsor, A., Jackson, A. P., Marino, S., & Shannon, A. 2017, MNRAS, 464, 3385
Yu, J., Huber, D., Bedding, T. R., & Stello, D. 2018, MNRAS, 480, L48
Ziegler, C., Law, N. M., Morton, T., et al. 2017, AJ, 153, 66